catalysts

MDPI

Article

Preparation and High-Throughput Testing of TiO_2-Supported Co Catalysts for Fischer-Tropsch Synthesis

Christian Schulz [1], Peter Kolb [1], Dennis Krupp [1], Lars Ritter [1], Alfred Haas [1], Mario Soorholtz [1], Thomas Emmerich Maldonado [2], Tobias Benjamin Thiede [2] and Carsten Knobloch [1,*]

[1] hte GmbH, the high throughput experimentation company, Kurpfalzring 104, 69123 Heidelberg, Germany; christian.schulz@hte-company.de (C.S.); peter.kolb@hte-company.de (P.K.); dennis.krupp@hte-company.de (D.K.); lars.ritter@hte-company.de (L.R.); alfred.haas@hte-company.de (A.H.); mario.soorholtz@basf.com (M.S.)

[2] Venator Germany GmbH, Dr.-Rudolf-Sachtleben-Straße 4, 47198 Duisburg, Germany; thomas_emmerich_maldonado@venatorcorp.com (T.E.M.); tobias_thiede@venatorcorp.com (T.B.T.)

* Correspondence: carsten.knobloch@hte-company.de; Fax: +49-06221-7497-137

Abstract: A series of Co/TiO_2 catalysts was tested in a parameters field study for Fischer-Tropsch synthesis (FTS). All catalysts were prepared by the conventional impregnation technique to obtain an industrially relevant Co content of 10 wt % or 20 wt %, respectively. In summary, 10 different TiO_2 of pure anatase phase, pure rutile phase, as well as mixed rutile and anatase phase were used as supports. Performance tests were conducted with a 32-fold high-throughput setup for accelerated catalyst benchmarking; thus, 48 experiments were completed within five weeks in a relevant operation parameters field (170 °C to 233.5 °C, H_2/CO ratio 1 to 2.5, and 20 bar(g)). The most promising catalyst showed a CH_4 selectivity of 5.3% at a relevant CO conversion of 60% and a C_{5+} productivity of 2.1 $g_{C5+}/(g_{Co}$ h) at 207.5 °C. These TiO_2-based materials were clearly differentiated with respect to the application as supports in Co-catalyzed FTS catalysis. The most prospective candidates are available for further FTS optimization at a commercial scale.

Keywords: high-throughput testing; parameters field study; Fischer–Tropsch synthesis; cobalt; TiO_2

check for updates

Citation: Schulz, C.; Kolb, P.; Krupp, D.; Ritter, L.; Haas, A.; Soorholtz, M.; Emmerich Maldonado, T.; Thiede, T.B.; Knobloch, C. Preparation and High-Throughput Testing of TiO_2-Supported Co Catalysts for Fischer-Tropsch Synthesis. *Catalysts* **2021**, *11*, 352. https://doi.org/10.3390/catal11030352

Academic Editors: Vladimir Mordkovich and Leonarda Liotta

Received: 29 January 2021
Accepted: 2 March 2021
Published: 9 March 2021

Publisher's Note: MDPI stays neutral with regard to jurisdictional claims in published maps and institutional affiliations.

Copyright: © 2021 by the authors. Licensee MDPI, Basel, Switzerland. This article is an open access article distributed under the terms and conditions of the Creative Commons Attribution (CC BY) license (https://creativecommons.org/licenses/by/4.0/).

1. Introduction

The mitigation of climate change and reduction of CO_2 emissions are urgent topics on the political agenda. In 2019, the European Union passed its vision of a sustainable economy by presenting "The European Green Deal" [1]. The main goal is to achieve climate neutrality by 2050. Prior to this, other nations had joined together and signed the Paris Agreement aiming to tackle the threat of climate change by keeping global temperature rise this century below 2 °C above pre-industrial levels [2]. Therefore, significant changes in the chemical industries are ongoing [3–5]. Some companies are already expecting the end of oil-driven growth and are changing their strategy [6,7]. The raw material bases of coal, oil, or gas are expected to shift to more sustainable ones such as renewable feedstocks as well as the utilization of CO_2.

Melero et al. 2012 described the challenges and early state-of-the-art of the bio-refinery in comparison to the petroleum refinery [8]. Although the topic is intensively studied, process development and catalyst optimization are still at an early stage [9]. In particular, the availability of bio-based feeds and optimized catalysts that are suited for diverse feeds is still not sufficient [10].

Another promising approach might be the conversion of synthesis gas generated via carbon-neutral routes with established processes. Sustainable generation of synthesis gas, i.e., a mixture of CO, CO_2, H_2, and steam, may be possible via various routes, e.g., gasification of biomass or municipal waste [11,12], or the conversion of CO_2 via reverse water–gas shift reaction with renewable H_2 [13].

Fischer–Tropsch synthesis (FTS) is an established process [14,15]. Typically, synthesis gas is generated from natural gas, and the subsequent FTS can be carried out in a low or high temperature range [16]. Brief information about both processes is summarized in Table 1.

Table 1. Overview Fischer-Tropsch synthesis (FTS) applications in industry.

Process	Low-Temperature FTS	High-Temperature FTS
Reaction temperature	220 to 240 °C	300 to 350 °C
Catalyst	Co-based	Fe-based
Product	Paraffins, long chains/waxes	Olefins, short chains, gasoline, chemicals
Reactor Type	Fixed bed, slurry bubble column	Fluidized bed reactors

FTS is strongly exothermic [15]. The reaction can be described via the simplified reaction equation Equation (1).

$$n\,CO + 2n\,H_2 \rightarrow (-CH_2-)_n + n\,H_2O \quad \Delta_R H_0(250\,^\circ C) = -158.5\,kJ/mol \tag{1}$$

Nevertheless, the product spectrum is more complex and the main products are straight-chain paraffins, olefins, and alcohols. Branched hydrocarbons and other oxygenates can also be formed, but in lower amounts. The oxygen is rejected as water or, for shift-active catalysts, also as CO_2.

Catalysts for FTS typically comprise Ni, Fe, Co, and Ru as the active component [16–20]. It is known that Ni generally leads to a very high CH_4 formation, which is undesirable, and that Ru shows good activity an selectivity but is expensive, which prohibits commercial use. Instead, Fe and Co are typically used for large-scale application. Carrier materials should be porous materials with a large specific surface area, enabling high dispersion of the active components. The interaction between active component and carrier should minimize sintering, which would lead to a loss in activity. Typical carrier materials are SiO_2, Al_2O_3, and TiO_2 [21–24].

However, to mitigate CO_2 emissions, it may be necessary to develop new processes and catalysts that are able to operate under conditions different from established processes. Furthermore, new processes may be tailored for a certain product spectrum. Due to the timeframe set by politics, a fast and cost-efficient way to perform catalyst research is necessary. High-throughput experimentation is one way to facilitate this task. This work demonstrates the application of high-throughput testing in the FTS of a supported Co catalyst on different TiO_2 supports.

2. Results and Discussion

2.1. Characterization of Materials

The support materials were prepared by a commercial process. They were first calcined at 350 °C prior to analysis by X-ray diffraction. Analysis of the phase composition via XRD shows that most materials exclusively consist of anatase phase TiO_2 with slightly varying crystallite sizes and typical reflections at 2θ = 25°, 38°, 48°, 55°, and 62.5°, corresponding to 101, 004, 200, 211, and 204 planes, respectively (Figure 1) [25–27]. TiO_2 #2 and #4 consist of pure rutile phase with typical reflections at 2θ = 27°, 36°, and 55°, corresponding to 110, 101, and 211 planes [25–27]. In contrast, TiO_2 #5 shows reflexes of both anatase and rutile phases. None of the powder XRD patterns indicate the presence of crystalline impurities.

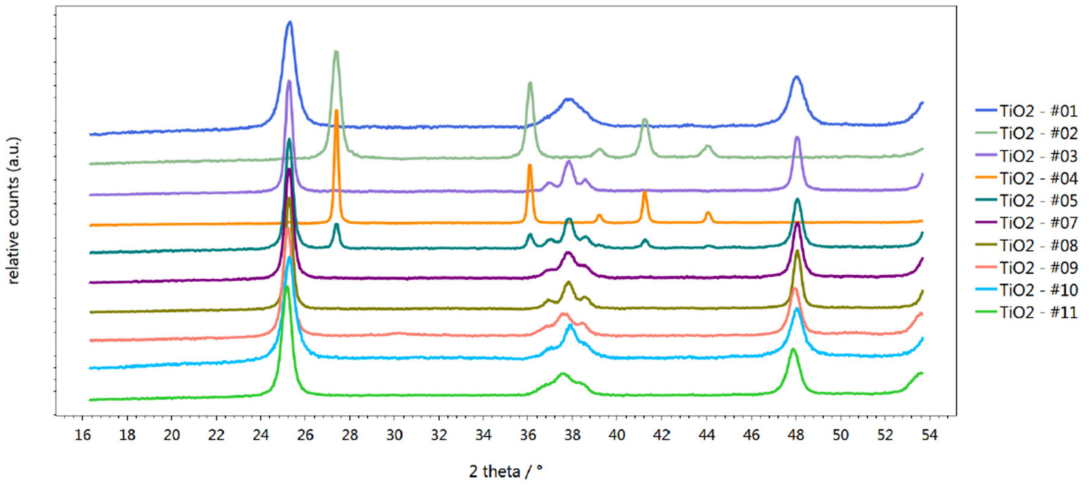


Figure 1. XRD pattern of investigated TiO_2 support materials.

For all 11 carriers, the specific surface areas were measured, both before and after impregnation with Co. The pure rutile carrier is essentially non-porous (<10 m^2/g). The mixed rutile/anatase phase had a much larger surface area of nearly 50 m^2/g, but all pure anatase-based materials had even larger surface areas of up to 158 m^2/g.

After impregnation, the surface areas of the materials were generally found to be lower than those of the pure carriers, which can be explained by the blocking of micropores. This effect is especially pronounced for the materials with higher Co loading. Moreover, the surface area loss is greater for high surface areas. An exception is the essentially non-porous carrier #4. For this material, an increase in surface area was observed after impregnation and calcination. This is most likely the result of changes in the textural properties, e.g., surface enhancement induced by nanoparticles. XRD and N_2 physisorption results are summarized in Table 2.

Table 2. Overview of supported Co catalysts on different TiO_2 supports.

Sample Description	Specific Surface Area of Support m^2/g	Co Loading/wt %	Specific Surface Area of Impregnated Support/m^2/g	Phase Composition of TiO_2
10 wt % Co/TiO_2—#01	158.9	10	100.6	Anatase
10 wt % Co/TiO_2—#02	56.7	10	44.7	Rutile
10 wt % Co/TiO_2—#03	57.4	10	45.6	Anatase
10 wt % Co/TiO_2—#04	5.4	10	10.9	Rutile
10 wt % Co/TiO_2—#05	48.8	10	39.0	Anatase/Rutile
10 wt % Co/TiO_2—#07	75.6	10	64.3	Anatase
10 wt % Co/TiO_2—#08	53.1	10	47.5	Anatase
10 wt % Co/TiO_2—#09	55.0	10	52.1	Anatase
10 wt % Co/TiO_2—#10	111.4	10	62.5	Anatase
10 wt % Co/TiO_2—#11	76.8	10	67.1	Anatase
20 wt % Co/TiO_2—#01	158.9	20	59.2	Anatase
20 wt % Co/TiO_2—#05	48.8	20	29.2	Anatase/Rutile
20 wt % Co/TiO_2—#07	75.6	20	52.6	Anatase
20 wt % Co/TiO_2—#10	111.4	20	34.5	Anatase
20 wt % Co/TiO_2—#11	76.8	20	52.5	Anatase

All of the 10 wt % samples and some of the anatase-based materials covering the range of surface areas were analyzed by XRD (Figure 2). The main reflex for Co_3O_4 can be found at approximately 2θ = 37°; however, the reflex is relatively broad, as the absence of sharp Co_3O_4 reflexes for all samples indicates that Co_3O_4 is finely dispersed within the sample.

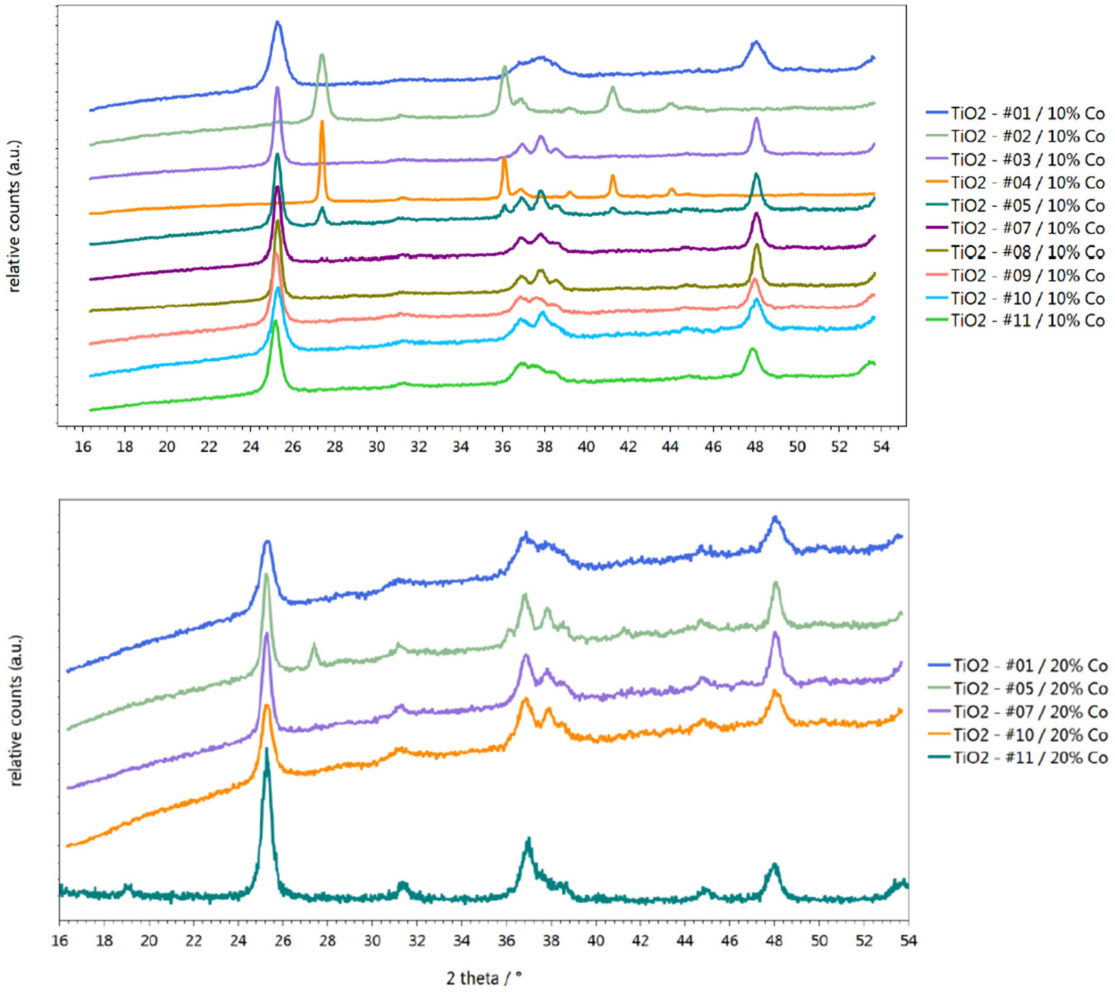


Figure 2. XRD analysis of Co supported on TiO_2 with 10 wt % (top) and 20 wt % (bottom) Co loading.

Reduction studies with temperature programmed reduction (TPR) showed the typical reduction profile for cobalt oxide clusters. The transformation of Co_3O_4 to CoO typically starts around 250 °C and is followed by the reduction of CoO to Co. The required temperature for the second reduction step depends on the support. The onset temperature can be found at approximately 350 °C. The final temperature for full conversion to metallic Co exceeds 600 °C for some materials (Figure 3). The results are in good agreement with the literature [21]. The reduction profiles of the carriers #1 and #10 are notably shifted to higher temperatures compared to the material #5 (Figure 3). This can be explained with higher dispersions of the Co in the high surface area supports TiO_2—#01 and TiO_2—#10 compared to the lower surface area TiO_2—#05 and resulting stronger metal support interaction. It is well known that the type of support has a pronounced influence on the reduction temperature and percentage reduction of cobalt clusters [28]. For the activation of the prepared catalysts, a maximum temperature of 350 °C was applied. Since all carriers had already been calcined at this temperature, phase transformation or changes in the material during catalyst activation are unlikely.

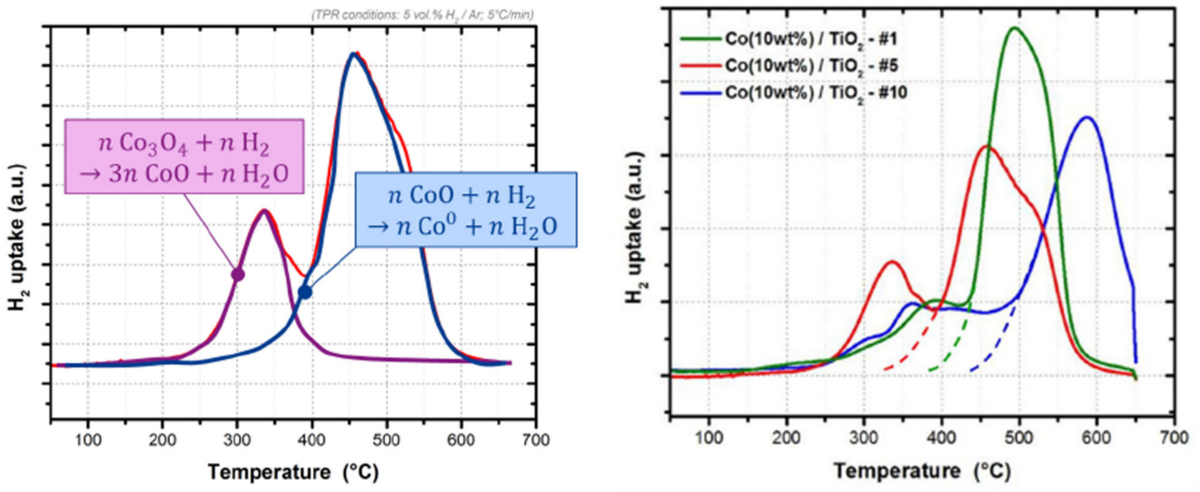


Figure 3. TPR experiment with two-step reduction of cobalt oxide (left). TPR experiments of cobalt oxide reduction on different support materials (right).

2.2. Performance Testing in FTS

After calcination of the materials, a defined fraction was loaded into the tubular reactors. Materials were reduced in situ by a mixture of 5 vol % H_2 in Ar. Synthesis gas was added at low temperature (150 °C) to avoid strong initial exothermal reactions, which would lead to sintering of the reduced Co particles. After a short stabilization time, the temperature was gradually increased, and reaction parameters were varied. An overview of all conditions is shown in Figure 4.

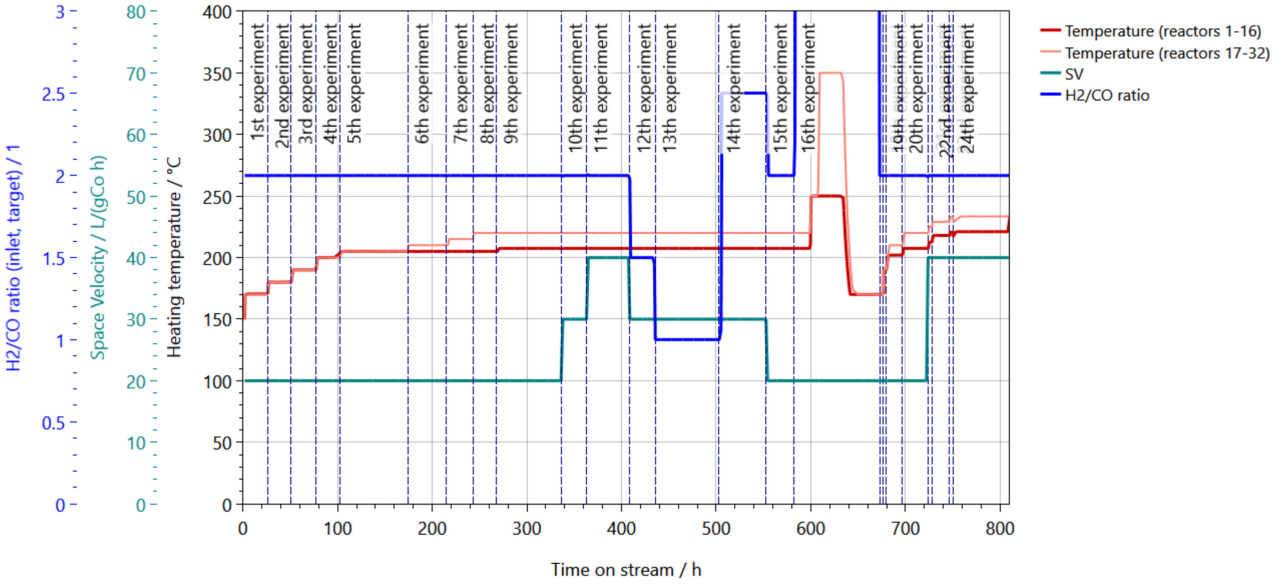


Figure 4. Overview of all applied reaction conditions.

At a temperature of 170 °C, the catalysts started to show a noticeable CO conversion. Catalysts based on support #01 and #10 showed negligible conversion. Based on the TPR result, this is attributed to incomplete reduction to elemental Co at 350 °C. Virtually no run-in behavior could be observed after a condition change, and the catalysts quickly reached a steady activity level.

Figure 5 shows the CO conversion data measured during experiment 5, i.e., at 200 °C and a space velocity (SV) of 20,000 as a function of the specific surface area of the impreg-

nated catalysts. Only materials with 10 wt % Co loading and a total amount of Co of 80 mg are considered. It can be seen that the most active materials with a CO conversion of >40% all have a surface area of >45 m^2/g. However, the material based on carrier #3 with a similar surface area is much less active (<5% CO conversion), and the material with the lowest surface area based on carrier #4 shows a moderate activity level. Shimura at al. have prepared a series of Co-based FT catalysts on TiO_2 supports that are modified with various metal ions [29]. Among the five unmodified materials, they found a maximum activity for a rutile-based carrier with a surface area of 33 m^2/g. However, the material had the highest surface area of Co. The surface area is clearly only one of several parameters that define the catalytic activity. A further analysis of the materials prepared in this study could help to better understand the property–activity relationships.

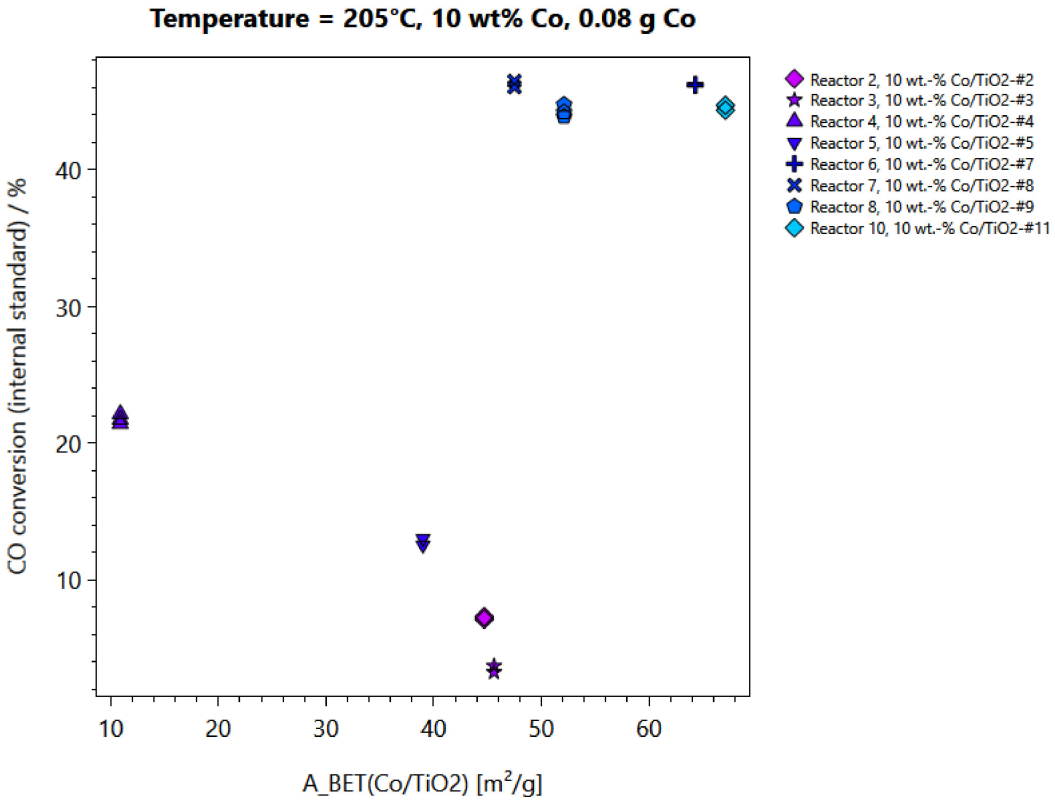


Figure 5. Correlation of specific surface area and conversion of CO.

Figure 6 shows the Arrhenius plots of the catalysts with support #07, #08, #09, and #11. An activation energy of approximately 120 kJ/mol can be derived. Similar values have been obtained for other catalysts [30,31].

The conversion of CO correlates with catalyst mass, space time velocity (GHSV), and temperature. For a better performance comparison, a modification of the gas hourly space-time velocity is defined per gram of metallic Co (GHSV=mL/(g_{Co} h)). Dependence on temperature is shown in Figure 7. Correlation of active mass with conversion is non-linear, and higher weights of the catalysts lead to higher conversion per weight unit, which can be explained by heat transport limitations of higher catalyst mass, i.e., local hot spots.

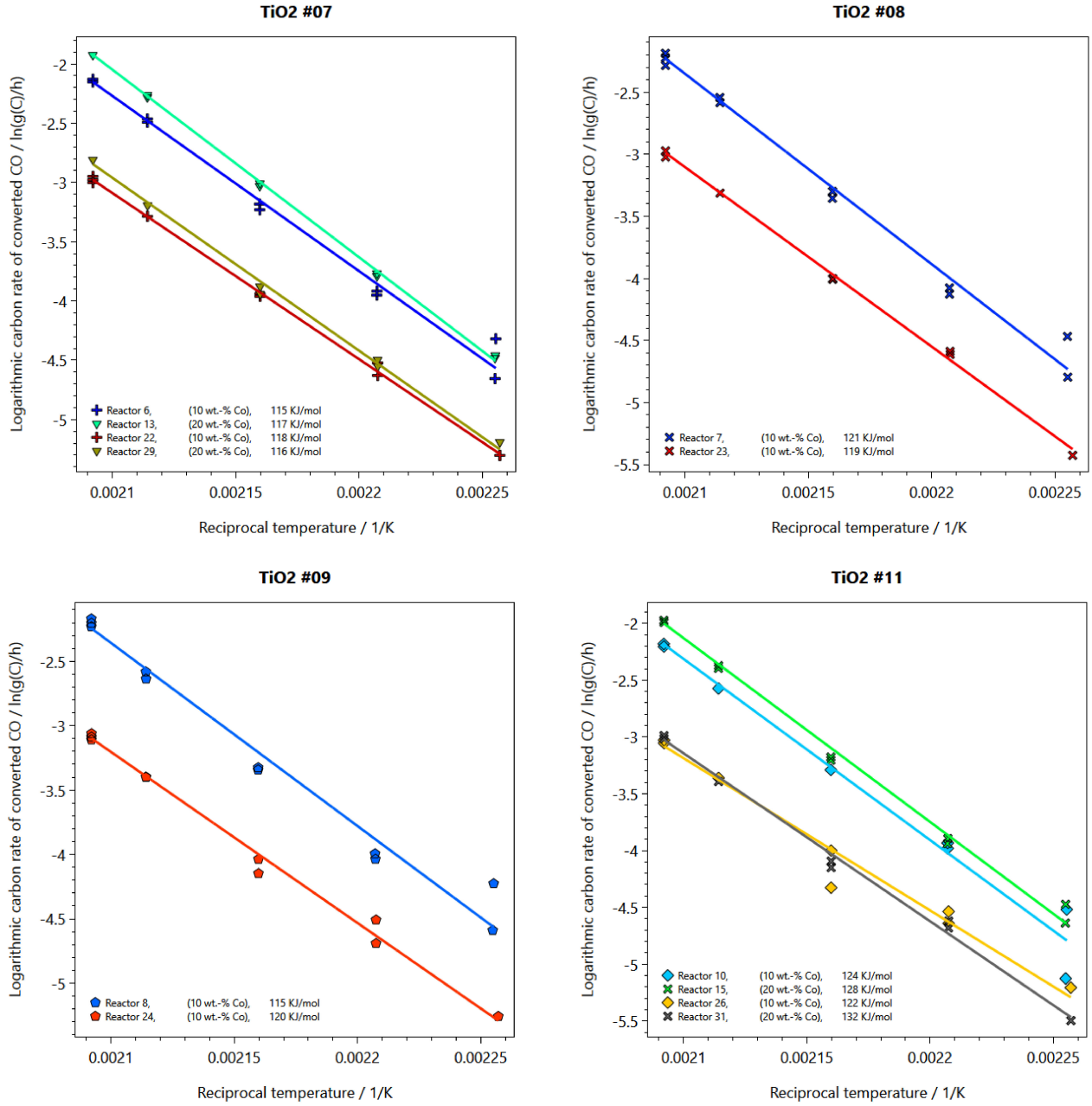


Figure 6. Arrhenius plots.

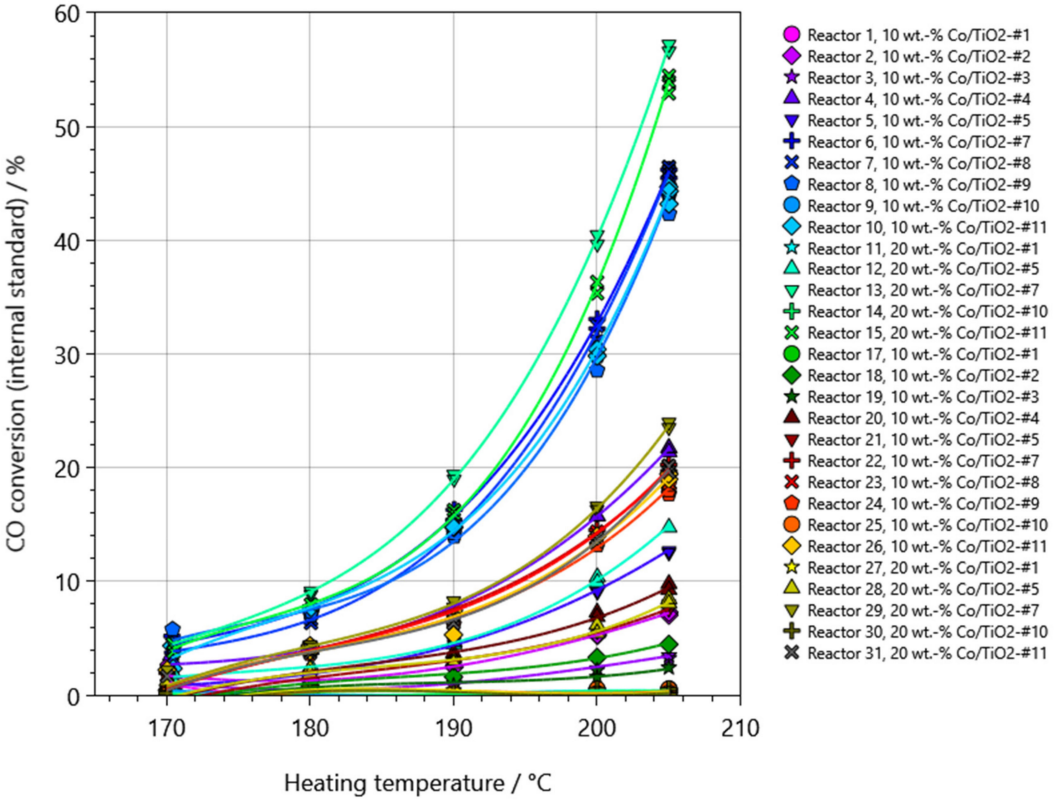


Figure 7. Conversion of CO as a function of reactor temperature.

In terms of commercial relevance, CH_4 selectivity and C_{5+} productivity are performance descriptors of interest. For a fair comparison between individual catalysts, they should be operated in a similar CO conversion range. This could be achieved by operating the catalyst with a Co loading of 80 mg at 207.5 °C, and those catalysts with a lower Co loading of 40 mg and thus a two times higher space velocity at a higher temperature of 220 °C. The conditions were chosen to achieve an industrially relevant CO conversion of approximately 60%. An overview of CH_4 selectivity and C_{5+} productivity as a function of CO conversion is given in Figure 8.

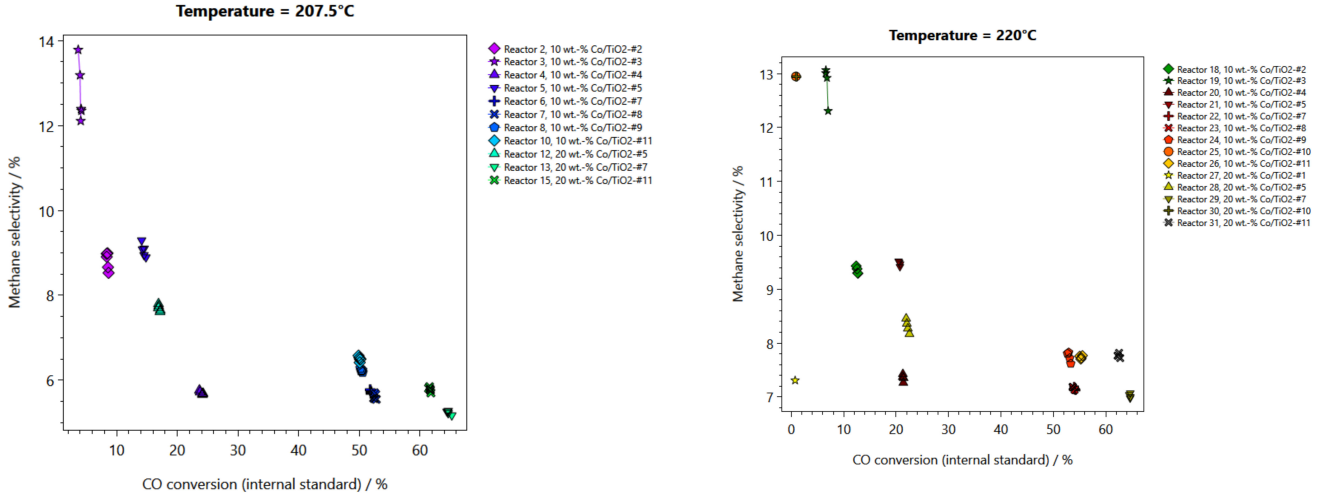


Figure 8. *Cont.*

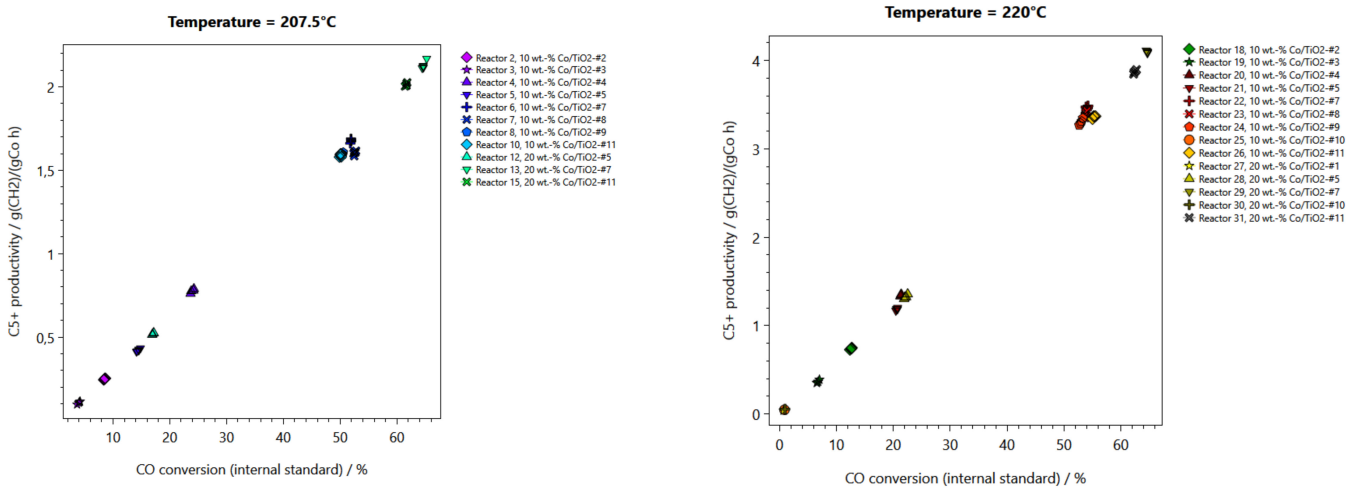


Figure 8. CH_4 selectivity and C_{5+} productivity of all catalysts for two experimental conditions.

Among the products in FTS, CH_4 is the least useful due to the high H_2 consumption in its production and the fact that it is the common starting material for the production of the synthesis gas. Thus, a low selectivity to CH_4 is a very desirable property of an FTS catalyst. In general, CH_4 selectivities up to 5% are regarded as "low". In the benchmarking tests, the lowest selectivity for CH_4 was 5.3% (20 wt % Co/TiO_2 support #7) and went up to only 6.6% for catalysts with support #04, #07, #08, #09, and #11 at 207.5 °C and 20 wt % Co. The other materials at identical temperature showed a significantly higher selectivity for CH_4 of up to 13.8%. At a higher temperature, the selectivity of CH_4 increased in most cases, and the lowest CH_4 selectivity observed was 7.1%. In general, the lowest CH_4 selectivities can be found at high conversion, indicating that the differences in the properties of the carrier and the preparation variables influence the chain growth and the CH_4 formation in different ways. High C_{5+} productivities were found. The best performance was reached with high Co loading of 20 wt % on support #7. At 207.5 °C, liquid productivities of 2.1 $g_{C5+}/(g_{Co}\ h)$ were found. By increasing the temperature to 220 °C and doubling the GHSV, the productivities increased to 4.1 $g_{C5+}/(g_{Co}\ h)$. Based on the catalyst volume, productivity of approximately 1,2 $g_{C5+}/(mL_{Cat}\ h)$ can be calculated. These values are in quite good accordance with literature values, e.g., Tonkovich et al. 2011 [32]. They performed a long-term stability test in a microchannel reactor with highly active Co-based catalysts. By varying GHSV to 80,000 $mL/(g_{Co}\ h)$ at 233.5 °C, the C_{5+} productivities can be maximized to 8.3 $g_{C5+}/(g_{Co}\ h)$. However, the selectivity for CH_4 is also increased to 9.5%.

Chain growth probability was determined by offline analysis of equilibrated wax samples for the described benchmarking conditions and selected positions. The fit was done between C_{30} and C_{40} hydrocarbons and yielded $0.86 < \alpha < 0.91$, which is expected for a Co-based catalyst.

In heterogeneously catalyzed reactions, the lifetime of the catalyst is a very important factor. Long lifetimes reduce the number of catalyst exchanges, which in turn leads to lower cost for a given catalyst and also reduces unproductive idle time during catalyst exchange. For FTS catalysts, lifetimes of years are desirable, which is partly due to the fact that Co is a relatively expensive metal. Tests to establish the long-term stability of FTS catalysts are normally performed by experiments under constant conditions lasting weeks and months. Due to the very limited testing time, the stability was probed by repeating a start-of-run condition at medium severity at the end of the run (CO conversion of best catalyst between 50% and 60%, 205 °C, 20 bar(g), H_2/CO ratio 2, 20,000 $mL/(g_{Co}\ h)$, 10 vol % Ar in feed). Within the initial experiments, no deactivation could be observed. Accelerated deactivation can be simulated at higher severity, i.e., higher conversion of CO and greater productivity. Therefore, higher reaction temperatures (221 °C and 233.5 °C, 20 bar(g), H_2/CO ratio 2,

40,000 mL/(g_{Co} h)) leading to CO conversion of up to 80% were tested. Under this chosen condition, significant deactivation was observed with a relative decrease of up to 25%, as shown in Figure 9.

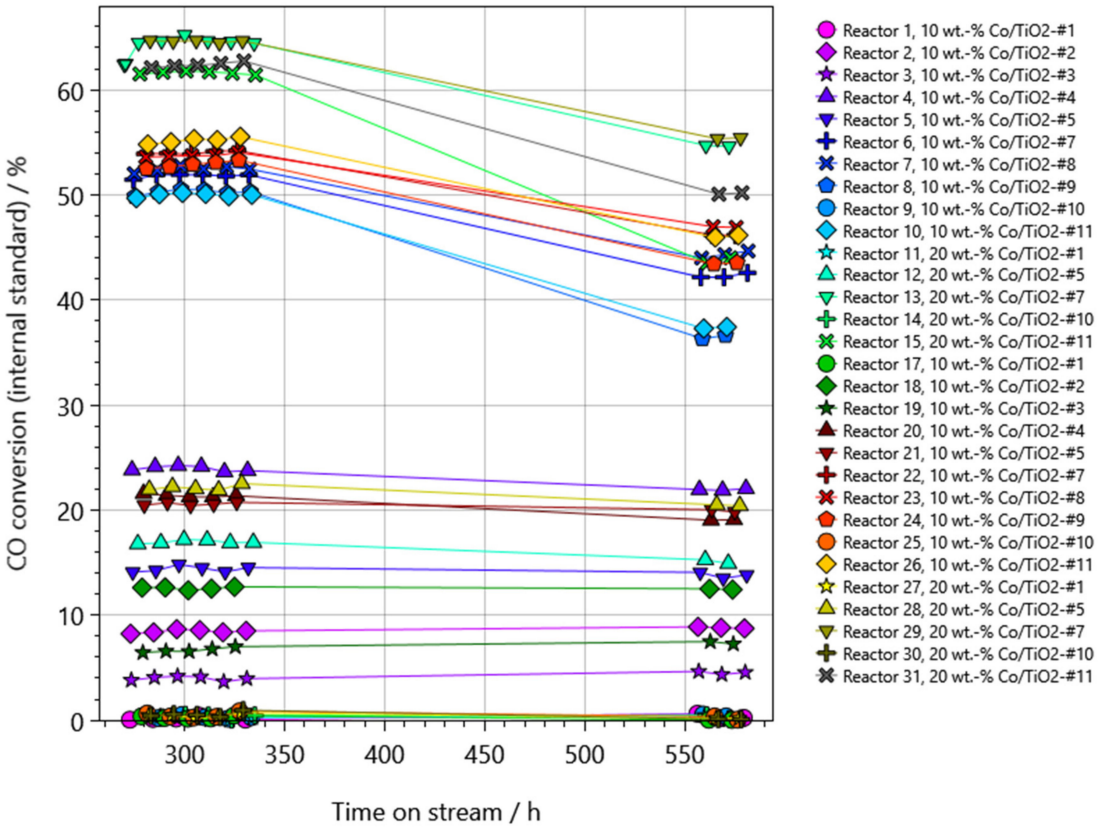


Figure 9. Catalyst deactivation after high severity experiments.

The high CO conversion leads to a high partial pressure of water, which, in combination with the high temperatures, leads to several deactivation processes such as hydrothermal sintering of Co particles, oxidation of active Co^0 to CoO, as well as the formation of Co-support compounds, which were recently found via in situ characterization published by Wolf et al. [33].

It is known in the literature that H_2-lean conditions can be correlated with catalyst deactivation by carbon formation on the catalyst [34]. Different carbon species are coke, Boudouard carbon, FTS intermediates or products, bulk carbide formation, polymeric carbon, and graphite [35,36]. It was speculated that the observed loss in activity might have been caused by an accumulation of long-chain hydrocarbons inside the pores or by coke deposition. In this case, treatment of the catalysts with pure H_2 can remove the deposits and restore the catalyst activity. Thus, the catalysts were treated with 90 vol % H_2 and 10 vol % Ar at a space velocity of 20,000 mL/(g_{Co} h) and a pressure of 20 bar(g). The temperature was 250 °C for reactor positions 1 to 16 and 350 °C for reactor positions 17 to 32 with a heating ramp of 1 K/min. Activity increased after H_2 treatment and was higher than expected. Indeed, after regeneration, most catalysts showed greater activity than observed at the start-of-run. Apparently, catalyst activation at the beginning did not fully reduce the cobalt oxides and the additional H_2 treatment has most likely generated additional Co^0 particles from previously unreduced Co oxide precursors.

In summary, this study demonstrates how high-throughput experimentation can be utilized to screen material libraries and identify promising catalytic lead materials. Activity, selectivity, and stability are investigated under industrially relevant conditions on a short time scale. Catalyst synthesis of 15 materials and 10 different TiO_2 supports was carried out

for four weeks, and benchmarking, regeneration tests, and stability tests were finished and evaluated within five weeks. Based on commercially available supports, catalyst libraries can be synthesized and tested for various applications in a short time frame.

However, this study shows only the first cycle in the development of new catalytic materials and the power of high-throughput testing can be unlocked through successive development cycles. An acceleration of catalyst and process development will be one key to overcoming the challenge of decarbonizing our society.

3. Experimental Section

3.1. Catalyst Preparation

All TiO_2 materials were received from Venator Germany GmbH. The materials were selected due to their different phase composition as well as specific surface area. All materials were calcined at 350 °C for six hours (heating ramp 1 K/min) in a constant flow of dried air using a conventional muffle oven. Each oxide support was compacted to tablets (13 mm diameter) using a hydraulic press and subsequently crushed and sieved in order to obtain a sufficient amount of particle size fraction in the range 125 to 160 µm.

For the modification of TiO_2 with Co (10 wt % Co), 5 g of TiO_2 was placed in a 50 mL flask to which was added a solution of $Co(NO_3)_2$ (Cobalt(II) nitrate hexahydrate; Acros Organics) in 30 mL of acetone. The mixture was vigorously shaken for one hour at high frequency using a lab shaker (CAT S20; 500 rpm; room temperature) in order to achieve complete wetting of the TiO_2 support and homogeneous distribution of the Co precursor. Subsequently, the sample was placed in a rotary evaporator and slowly heated up to a temperature of 55 °C. After approximately 30 minutes, the pressure was lowered to 550 mbar via a membrane pump. The sample was kept rotating for at least two hours until a dry, pinkish powder was obtained. Then, the dried and impregnated samples were placed in a muffle oven with a constant flow of air, heated up with 1 K/min to 350 °C, and kept at this temperature for six hours before the sample was allowed to cool down to room temperature.

Based on the highest specific surface area after impregnation, supports were chosen for a higher cobalt loading. For the modification of TiO_2 with Co (20 wt % Co), the same experimental procedure was used as for preparation of TiO_2 with Co (10 wt % Co). However, the procedure was optimized to avoid the decomposition of high amounts of nitrate precursors (e.g., in case of one-step impregnation of 20 wt % Co), which is generally considered to lead to larger agglomerates of metals or metal oxides. Thus, a significantly milder procedure was chosen for modification with Co. In particular, TiO_2 with Co (20 wt % Co) samples were prepared according to the following sequence:

i. Impregnation of TiO_2 with $Co(NO_3)_2$ (targeting 10 wt % Co)
ii. Drying and calcination as described above
iii. Impregnation of TiO_2 with $Co(NO_3)_2$ (targeting 15 wt % Co including the previous impregnation step)
iv. Drying and calcination as described above
v. Impregnation of TiO_2 with $Co(NO_3)_2$ (targeting 20 wt % Co including the previous two impregnation steps)
vi. Drying and calcination as described above

Finally, calcined samples were sieved to remove all potential fines from the particle size fraction 125 to 160 µm.

3.2. Catalyst Characterization

BET measurements were carried out in a volumetric N_2 physisorption setup (Autosorb-6-B, Quantachrome) at the temperature of liquid N_2. The sample was degassed in a dynamic vacuum at 150 °C for two hours prior to physisorption. Full adsorption–desorption isotherms were recorded. The specific surface area according to the BET method was calculated from the linear range of the adsorption isotherm (p/p_0 = 0.05 to 0.28). The catalyst was characterized before and after catalytic testing.

XRD measurements were performed in Bragg–Brentano reflection geometry on a theta/theta diffractometer (D8 Advance, Bruker AXS) equipped with a secondary graphite monochromator (Cu $K_{\alpha 1+2}$ radiation) and scintillation detector. Sample powder was filled into the recess of a cup-shaped sample holder, the surface of the powder bed being flush with the edge of the sample holder. Data analysis was performed using the software package Topas (v 2.1, Bruker AXS) [37].

Temperature-programmed reduction experiments were conducted inside a commercial device from Micromeritics. An oxidic form of selected catalytic material was loaded into the TPR setup. A flow of 5 vol % H_2 in Ar was passed over the sample with a heating ramp rate of 5 K/min.

3.3. High-Throughput Testing of Catalysts

The catalysts were loaded in the reactors on a wet basis, i.e., without previous drying. Corundum in 125 to 160 µm was used as the upper and post bed up front and below the catalyst bed. The same particle size was used in order to avoid mixing particles of different sizes. The catalyst beds were not diluted with inert material. The results described in this study were obtained from a single set of reactors. The details of the reactor filling are provided in Table 3.

Table 3. Reactor loading design for parallel testing.

Heating Block	Reactor Position	Sample Description	Co Loading / wt %	Support Number	Wet-Based Mass/g	Co Mass/mg
A	1	10 wt % Co/TiO_2—#01	10	1	0.807	80
	2	10 wt % Co/TiO_2—#02	10	2	0.807	80
	3	10 wt % Co/TiO_2—#03	10	3	0.809	80
	4	10 wt % Co/TiO_2—#04	10	4	0.808	80
	5	10 wt % Co/TiO_2—#05	10	5	0.807	80
	6	10 wt % Co/TiO_2—#07	10	7	0.808	80
	7	10 wt % Co/TiO_2—#08	10	8	0.809	80
	8	10 wt % Co/TiO_2—#09	10	9	0.809	80
	9	10 wt % Co/TiO_2—#10	10	10	0.808	80
	10	10 wt % Co/TiO_2—#11	10	11	0.807	80
	11	20 wt % Co/TiO_2—#01	20	1	0.404	80
	12	20 wt % Co/TiO_2—#05	20	5	0.404	80
	13	20 wt % Co/TiO_2—#07	20	7	0.405	80
	14	20 wt % Co/TiO_2—#10	20	10	0.403	80
	15	20 wt % Co/TiO_2—#11	10	11	0.405	80
	16	Inert	-	-	-	-
B	17	10 wt % Co/TiO_2—#01	10	1	0.405	40
	18	10 wt % Co/TiO_2—#02	10	2	0.404	40
	19	10 wt % Co/TiO_2—#03	10	3	0.404	40
	20	10 wt % Co/TiO_2—#04	10	4	0.405	40
	21	10 wt % Co/TiO_2—#05	10	5	0.405	40
	22	10 wt % Co/TiO_2—#07	10	7	0.404	40
	23	10 wt % Co/TiO_2—#08	10	8	0.403	40
	24	10 wt % Co/TiO_2—#09	10	9	0.403	40
	25	10 wt % Co/TiO_2—#10	10	10	0.403	40
	26	10 wt % Co/TiO_2—#11	10	11	0.405	40
	27	20 wt % Co/TiO_2—#01	20	1	0.203	40
	28	20 wt % Co/TiO_2—#05	20	5	0.201	40
	29	20 wt % Co/TiO_2—#07	20	7	0.201	40
	30	20 wt % Co/TiO_2—#10	20	10	0.203	40
	31	20 wt % Co/TiO_2—#11	20	11	0.201	40
	32	Inert	-	-	-	-

Catalytic tests were performed in a fully automated, commercial 32-fold parallel testing setup designed and built by hte GmbH. The gas-dosing unit provides mixed

feeds comprising H_2 (0 vol % to 70 vol %), CO (0 vol % to 50 vol %), and Ar (as an internal standard, 10 vol %). The typical range of gas hourly space velocities (GHSV) is 10,000–80,000 mL/(g_{Co} h). Catalyst volumes of up to 1 mL were placed inside stainless steel reactors with inner diameters of 6 mm. Before catalytic testing, isothermal zones were determined with stainless steel thermowells (1/8" outer diameter) in the center of all reactors. An isothermal zone was defined with a temperature deviation of ±1 K. In total, 32 reactors can be tested in parallel. The reactor unit comprises two separate slice reactor blocks, each designed for 16 reactors. The two reactor blocks can be individually temperature controlled up to 450 °C. The process control for equal feed distribution and constant reaction pressure is based on the technology described in the patent [38]. A simplified process scheme of the setup is shown in Figure 8 to reduce complexity; the degree of parallelization is reduced to 4 reactors in parallel (Figure 10).

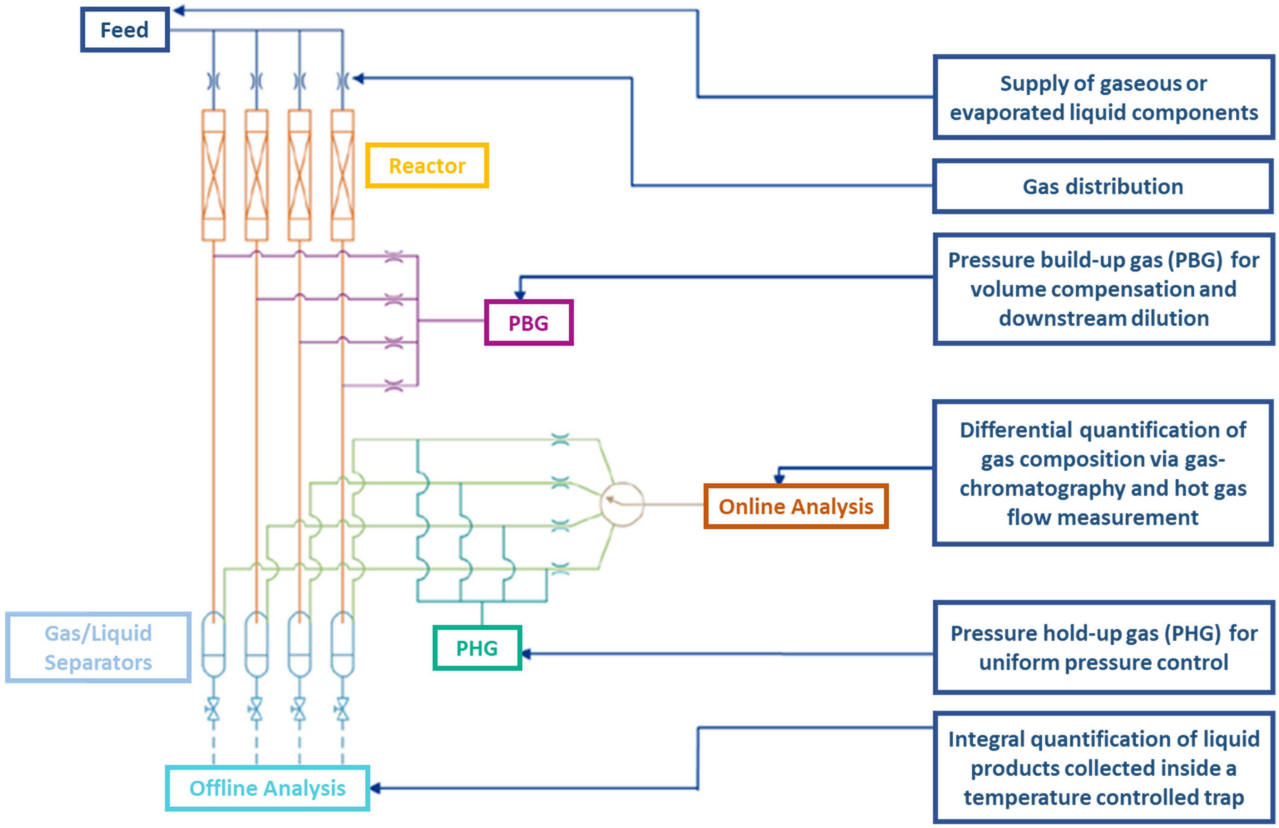


Figure 10. Simplified process scheme of a parallel test unit.

Using the parallel testing setup, the variation of space-time velocities was realized by loading the channels with different amounts of catalyst. The larger catalyst amounts were loaded in reactor heating block 1, while the smaller amounts (half the amount compared to reactor heating block 1) were loaded in reactor heating block 2.

The catalysts were dried under pure Ar (GHSV = 60,000 mL/(g_{Co} h) at 110 °C and 1 atm for two hours to purge the catalyst bed of air and residual moisture. The activation was performed with 25 vol % H_2 in Ar (GHSV = 60,000mL/(g_{Co} h) at 350 °C (1 K/min heating ramp) and 1 atm for 24 h. The chosen procedure is comparable to activation protocols from the literature [39].

Cooling to 150 °C after finishing catalyst activation was done in 100 vol % Ar without a defined temperature ramp. Afterward, the system was pressurized to 20 bar(g) with synthesis gas (H_2/CO ratio 2, Ar content 10 vol %). A full parameter field variation of temperature, GHSV, and H_2/CO ratio was applied to all 30 catalysts. An overview of all

reaction conditions can be found in Table 4. A detailed overview is shown in the Appendix A1.

Table 4. Overview of experimental conditions.

GHSV/mL/(g_{Co} h)	20,000 to 80,000
H_2/CO ratio	1 to 2.5
Internal standard Ar/vol %	10
Temperature/°C	150 to 233.5
p/bar(g)	20

Matching industrially relevant feed conditions, the sequence of catalytic testing comprises a temperature variation (170 to 233.5 °C), H_2/CO ratio adaption (1 to 2.5), and a GHSV variation (20,000 mL/(g_{Co} h) to 40,000 mL/(g_{Co} h)). The total gas pressure was kept constant at 20 bar(g) throughout the entire run. Each reactor was measured at least three times to check the time scale of equilibration required for stable catalytic performance. To monitor catalyst aging effects on activity and product selectivity, a reference point was measured (207.5 °C and 220 °C, H_2/CO ratio 2, 20,000 mL/(g_{Co} h)) after 24 days on stream.

The product gases are analyzed by two gas chromatographs (GC 7890 A, Agilent). Each GC is mounted with three detectors. In total, three flame ionization detectors (FID) and three thermal conductivity detectors (TCD) were utilized for a full gas-phase analysis up to C_{20}. The first FID is connected to an isomer resolving column for analysis of all isomers from C_1 to C_5. The second FID is connected to a boiling point column, where C_5 to C_{20} compounds are analyzed. The third FID is mounted with a Jetanizer for CO_x analytics. The first TCD is connected to a molecular sieve column and optimized for H_2 and N_2 analytics. The second TCD is used for Ar analysis as well as for CO_x. The last TCD can be used for water analysis. The effluent gas of the blank reactor, which has the same composition as the inlet gas, is also analyzed to verify the correct operation of the feed dosage and the analysis. Prior to the GC analysis, all effluent gas streams are diluted with hot inert gas to provide a defined cut of the gas phase products. Liquid products are separated inside a hot trap at 130 °C. Transfer lines between reactors and gas chromatographs are heated (200 °C). Before the GC, the hot gas flow (HGF) is measured with a flow indicator. Typically, gas-phase compositions up to C_{20} can be differentially analyzed in the gas phase via online GC and hot gas flow indicator, where longer hydrocarbons are integrally analyzed with offline methods. Therefore, the amount of wax is collected, and liquid samples are extracted via manual valves on the hot trap; then, they are quantified via mass balance. To avoid instationary composition, the wax formed initially at each condition is discarded and equilibrated wax composition is collected. The composition of the wax sample is analyzed via offline GC. The mass of the wax samples and its composition measured by offline gas chromatography is combined with the online gas chromatograms and process parameters measured during the sample collection. From the merged results, a full Schultz Flory distribution covering gas and liquid phase can be derived.

The conversion (X) of CO (Equation (2)) and the selectivities (S) of the respective products (Equation (3)) are calculated from the concentrations measured with reference to the internal standard Ar. The productivities of each product are calculated from the carbon concentrations referred to as CH_2 per loaded mass of metallic Co (Equation (4)).

$$X(CO) = 1\frac{A_{CO}}{A_{CO,0}} \times \frac{A_{Ar,0}}{A_{Ar}} \quad (2)$$

with A = area derived from GC chromatogram

$$S_i = \frac{cc_i \times HGF_i}{cc_{CO,0} \times HGF_0 \, x \, X(CO)} \quad (3)$$

with i = reaction products, cc = carbon concentration with (cc) = g_{Carbon}/L, with HGF = hot gas flow with (HGF) = L/h.

$$P_i = cc_i \times HGF / m_{Co} \quad (4)$$

with m = mass.

Author Contributions: Conceptualization, A.H. and C.K.; methodology, C.K.; validation, D.K., L.R. and C.K.; formal analysis, P.K.; investigation, M.S.; resources, T.E.M. and T.B.T.; data curation, C.S.; writing—original draft preparation, C.S.; writing—review and editing, C.S.; visualization, P.K.; supervision, A.H.; project administration, C.K.; funding acquisition, T.E.M. and T.B.T.. All authors have read and agreed to the published version of the manuscript.

Funding: This research received no external funding.

Data Availability Statement: 3rd Party Data: Restrictions apply to the availability of these data. Data was obtained from the GmbH and are available from Carsten Knobloch with the permission of Venator Germany GmbH.

Conflicts of Interest: The authors declare no conflict of interest.

Appendix A

Table A1. Detailed overview of experimental conditions.

Day	Experiment Number	Temperature (Reactor 1 to 16)/°C	Temperature (Reactor 17 to 32)/°C	Pressure/bar(g)	GHSV (Reactor 1 to 16)/mL/(g_{Co} h)	GHSV (Reactor 17 to 32)/mL/(g_{Co} h)	H_2/CO Ratio
1	1	170	170	20	20,000	40,000	2.0
2	2	180	180	20	20,000	40,000	2.0
3	3	190	190	20	20,000	40,000	2.0
4	4	200	200	20	20,000	40,000	2.0
5	5	205	205	20	20,000	40,000	2.0
8	6	205	210	20	20,000	40,000	2.0
10	7	205	215	20	20,000	40,000	2.0
11	8	205	220	20	20,000	40,000	2.0
12	9	207.5	220	20	20,000	40,000	2.0
15	10	207.5	220	20	20,000	40,000	2.0
16	11	207.5	220	20	40,000	80,000	2.0
18	12	207.5	220	20	30,000	60,000	1.5
19	13	207.5	220	20	30,000	60,000	1.0
22	14	207.5	220	20	30,000	60,000	2.5
24	15	207.5	220	20	20,000	40,000	2.0
25	16	250	350	20	20,000	40,000	n.a.
29	17	170	170	20	20,000	40,000	2.0
29	18	190	190	20	20,000	40,000	2.0
29	19	202	210	20	20,000	40,000	2.0
30	20	207.5	220	20	20,000	40,000	2.0
31	21	212.5	225	20	40,000	80,000	2.0
32	22	218	229	20	40,000	80,000	2.0
32	23	220.5	233	20	40,000	80,000	2.0
32	24	221	233.5	20	40,000/	80,000	2.0

References

1. Comm/dg/unit. A European Green Deal. Available online: https://ec.europa.eu/info/strategy/priorities-2019-2024/european-green-deal_en (accessed on 7 December 2020).
2. The Paris Agreement | UNFCCC. Available online: https://unfccc.int/process-and-meetings/the-paris-agreement/the-paris-agreement (accessed on 7 December 2020).
3. Kätelhön, A.; Meys, R.; Deutz, S.; Suh, S.; Bardow, A. Climate change mitigation potential of carbon capture and utilization in the chemical industry. *Proc. Natl. Acad. Sci. USA* **2019**, 11187–11194. [CrossRef]
4. Vogel, G.H. Change in Raw Material Base in the Chemical Industry. *Chem. Eng. Technol.* **2008**, *31*, 730–735. [CrossRef]
5. Pagliaro, M. An Industry in Transition: The Chemical Industry and the Megatrends Driving Its Forthcoming Transformation. *Angew. Chem. Int. Ed.* **2019**, 11154–11159. [CrossRef]
6. bp Global. Oil | Energy Economics | Home. Available online: https://www.bp.com/en/global/corporate/energy-economics/energy-outlook/demand-by-fuel/oil.html (accessed on 7 December 2020).
7. Shell's Ambition to Be a Net-Zero Emissions Energy Business. Available online: https://www.shell.com/energy-and-innovation/the-energy-future/shells-ambition-to-be-a-net-zero-emissions-energy-business.html (accessed on 10 January 2020).
8. Melero, J.A.; Iglesias, J.; Garcia, A. Biomass as renewable feedstock in standard refinery units. Feasibility, opportunities and challenges. *Energy Environ. Sci.* **2012**, *5*, 7393. [CrossRef]
9. Fernando, S.; Adhikari, S.; Chandrapal, C.; Murali, N. Biorefineries: Current Status, Challenges, and Future Direction. *Energy Fuels* **2006**, *20*, 1727–1737. [CrossRef]
10. Rauch, R.; Kiennemann, A.; Sauciuc, A. Fischer-Tropsch Synthesis to Biofuels (BtL Process). In *The Role of Catalysis for the Sustainable Production of Bio-Fuels and Bio-Chemicals*; Elsevier: Amsterdam, The Netherlands, 2013; pp. 397–443. [CrossRef]
11. Luo, S.; Zhou, Y.; Yi, C. Syngas production by catalytic steam gasification of municipal solid waste in fixed-bed reactor. *Energy* **2012**, *44*, 391–395. [CrossRef]
12. Arena, U. Process and technological aspects of municipal solid waste gasification. A review. *Waste Manag.* **2012**, *32*, 625–639. [CrossRef]
13. Daza, Y.A.; Kuhn, J.N. CO_2 conversion by reverse water gas shift catalysis: Comparison of catalysts, mechanisms and their consequences for CO_2 conversion to liquid fuels. *RSC Adv.* **2016**, *6*, 49675–49691. [CrossRef]
14. Rostrup-Nielsen, J.R. Syngas in perspective. *Catal. Today* **2002**, *71*, 243–247. [CrossRef]
15. Saeidi, S.; Talebi Amiri, M.; Saidina Amin, N.A.; Rahimpour, M.R. Progress in Reactors for High-Temperature Fischer–Tropsch Process: Determination Place of Intensifier Reactor Perspective. *Int. J. Chem. React. Eng.* **2014**, *12*, 639–664. [CrossRef]
16. Mahmoudi, H.; Mahmoudi, M.; Doustdar, O.; Jahangiri, H.; Tsolakis, A.; Gu, S.; LechWyszynski, M. A review of Fischer Tropsch synthesis process, mechanism, surface chemistry and catalyst formulation. *Biofuels Eng.* **2017**, *2*, 11–31. [CrossRef]
17. Ponec, V. Some Aspects of the Mechanism of Methanation and Fischer-Tropsch Synthesis. *Catal. Rev.* **1978**, *18*, 151–171. [CrossRef]
18. Jager, B.; Espinoza, R. Advances in low temperature Fischer-Tropsch synthesis. *Catal. Today* **1995**, *23*, 17–28. [CrossRef]
19. Yang, J.; Ma, W.; Chen, D.; Holmen, A.; Davis, B.H. Fischer–Tropsch synthesis: A review of the effect of CO conversion on methane selectivity. *Appl. Catal. A Gen.* **2014**, *470*, 250–260. [CrossRef]
20. Van der Laan, G.P.; Beenackers, A.A.C.M. Kinetics and Selectivity of the Fischer–Tropsch Synthesis: A Literature Review. *Catal. Rev.* **1999**, *41*, 255–318. [CrossRef]
21. Viswanathan, B.; Gopalakrishnan, R. Effect of support and promoter in Fischer-Tropsch cobalt catalysts. *J. Catal.* **1986**, *99*, 342–348. [CrossRef]
22. Borg, Ø.; Eri, S.; Blekkan, E.A.; Storsæter, S.; Wigum, H.; Rytter, E.; Holmen, A. Fischer–Tropsch synthesis over γ-alumina-supported cobalt catalysts: Effect of support variables. *J. Catal.* **2007**, *248*, 89–100. [CrossRef]
23. Bessel, S. Support effects in cobalt-based Fischer-Tropsch catalysis. *Appl. Catal. A Gen.* **1993**, *96*, 253–268. [CrossRef]
24. Jacobs, G.; Das, T.K.; Zhang, Y.; Li, J.; Racoillet, G.; Davis, B.H. Fischer–Tropsch synthesis: Support, loading, and promoter effects on the reducibility of cobalt catalysts. *Appl. Catal. A Gen.* **2002**, *233*, 263–281. [CrossRef]
25. Sakurai, K.; Mizusawa, M. X-ray diffraction imaging of anatase and rutile. *Anal. Chem.* **2010**, *82*, 3519–3522. [CrossRef] [PubMed]
26. Peng, B.; Meng, X.; Tang, F.; Ren, X.; Chen, D.; Ren, J. General Synthesis and Optical Properties of Monodisperse Multifunctional Metal-Ion-Doped TiO 2 Hollow Particles. *J. Phys. Chem. C* **2009**, *113*, 20240–20245. [CrossRef]
27. Yan, Z.; Wu, H.; Han, A.; Yu, X.; Du, P. Noble metal-free cobalt oxide (CoO) nanoparticles loaded on titanium dioxide/cadmium sulfide composite for enhanced photocatalytic hydrogen production from water. *Int. J. Hydrogen Energy* **2014**, *39*, 13353–13360. [CrossRef]
28. Reuel, R. Effects of support and dispersion on the CO hydrogenation activity/selectivity properties of cobalt. *J. Catal.* **1984**, *85*, 78–88. [CrossRef]
29. Shimura, K.; Miyazawa, T.; Hanaoka, T.; Hirata, S. Fischer–Tropsch synthesis over TiO_2 supported cobalt catalyst: Effect of TiO_2 crystal phase and metal ion loading. *Appl. Catal. A Gen.* **2013**, *460–461*, 8–14. [CrossRef]
30. Post, M.F.M.; Van't Hoog, A.C.; Minderhoud, J.K.; Sie, S.T. Diffusion limitations in fischer-tropsch catalysts. *AICHE J.* **1989**, *35*, 1107–1114. [CrossRef]

31. Lyu, S.; Wang, L.; Zhang, J.; Liu, C.; Sun, J.; Peng, B.; Wang, Y.; Rappé, K.G.; Zhang, Y.; Li, J.; et al. Role of Active Phase in Fischer–Tropsch Synthesis: Experimental Evidence of CO Activation over Single-Phase Cobalt Catalysts. *ACS Catal.* **2018**, *8*, 7787–7798. [CrossRef]
32. Jarosch, K.T.; Tonkovich, A.L.Y.; Perry, S.T.; Kuhlmann, D.; Wang, Y. Microchannel Reactors for Intensifying Gas-to-Liquid Technology. In *Microreactor Technology and Process Intensification*; ACS Symposium Series; ACS: Washington, DC, USA, 2005; pp. 258–272. [CrossRef]
33. Wolf, M.; Fischer, N.; Claeys, M. Water-induced deactivation of cobalt-based Fischer–Tropsch catalysts. *Nat. Catal.* **2020**, *3*, 962–965. [CrossRef]
34. Tsakoumis, N.E.; Rønning, M.; Borg, Ø.; Rytter, E.; Holmen, A. Deactivation of cobalt based Fischer–Tropsch catalysts: A review. *Catal. Today* **2010**, *154*, 162–182. [CrossRef]
35. Bartholomew, C.H. Carbon Deposition in Steam Reforming and Methanation. *Catal. Rev.* **1982**, *24*, 67–112. [CrossRef]
36. Moodley, D.J. On the deactivation of cobalt-based Fischer-Tropsch synthesis catalysts. *Am. Chem. Soc. Div. Petrochem. Chem.* **2008**, *53*, 122–125.
37. Snyder, R.L.; Fiala, J.; Bunge, H.-J. *Defect and Microstructure Analysis by Diffraction*; Oxford Science Publications: Oxford, UK; Oxford University Press: Oxford, UK, 1999; Volume 10.
38. Brenner, A.; Friess, M.; Haas, A.; Köchel, O.; Strehlau, W.; Zech, T. Device and Method for Pressure and Flow Control in Parallel Reactors. Patent PCT/EP2004/014509, 23 December 2003.
39. Eschemann, T.O.; Oenema, J.; de Jong, K.P. Effects of noble metal promotion for Co/TiO_2 Fischer-Tropsch catalysts. *Catal. Today* **2016**, *261*, 60–66. [CrossRef]